IEEE Access
Multidisciplinary | Rapid Review | Open Access Journal

Received August 25, 2019, accepted September 15, 2019, date of publication September 27, 2019, date of current version October 9, 2019.

Digital Object Identifier 10.1109/ACCESS.2019.2944160

A Flexible Collision Avoidance Strategy for the Formation of Multiple Unmanned Aerial Vehicles

XU ZHU, YUFEI LIANG, AND MAODE YAN
School of Electronic and Control Engineering, Chang'an University, Xi'an 710064, China

Corresponding author: Yufei Liang (yufeiliang@chd.edu.cn)

This work was supported in part by the National Natural Science Foundation of China under Grant 61803040, in part by the China Postdoctoral Science Foundation under Grant 2017M613030, and in part by the Special Fund for Basic Scientific Research of Central Colleges under Grant 300102328403.

ABSTRACT This paper develops a flexible collision avoidance strategy for the formation of multiple unmanned aerial vehicles (multi-UAV). Firstly, To make full use of the information flow from the communication of the formation, an improved artificial potential field (IAPF) function is constructed by adding the communication topology and communication weights. Based on the IAPF functions, both collision avoidance within the formation and obstacle avoidance outside the formation are well organized to ensure flight safety. Secondly, to fuse collision avoidance and formation keeping, we design the null space behavioral (NSB) approach to combine them into a single motion command, where the formation keeping algorithm is designed as a second-order consensus algorithm. In this way, the flexible collision avoidance strategy is proposed based on IAPF and consensus, handling the relationship between collision avoidance and formation keeping flexibly. Finally, three-dimensional multi-UAV flight simulation validates the effectiveness of the proposed strategy that the formation can both implement collision avoidance quickly and keep a good geometric formation configuration simultaneously.

INDEX TERMS Unmanned aerial vehicle, collision avoidance, formation keeping, improved artificial potential field, null space behavioral.

I. INTRODUCTION

The formation of multiple unmanned aerial vehicles (multi-UAV) has traditionally been used in military operations for a number of years [1]. Recently, it has generated a lot of interests due to its potential application in civilian domains such as emergency management, law enforcement, precision agriculture, package delivery, and imaging/surveillance [2], [3]. Owing to higher efficiency and less fuel consumption, the formation of multi-UAV has unique advantages over a single UAV, therefore it has good prospects in both military and civilian fields.

In the formation of multi-UAV, collision avoidance is quite essential, which is directly related to flight safety. In other words, any two UAVs should maintain a certain distance to ensure the safety [4]. Besides, there are obstacles threatening flight safety outside the formation [5]. For these two reasons, increasing research attention has been paid to the collision avoidance algorithms [6]–[12].

Basically, in the literature, there are generally four research methods about collision avoidance, namely artificial potential field (APF) [13], geometric method [14], gridding approach [15], and genetic algorithm [16]. Thereinto, APF is the most frequently-used collision avoidance method thanks to its mathematical elegance and simplicity, and it is especially suitable for real-time collision avoidance [17]. In the APF method, both the repulsive potential field and attractive potential field work together to ensure an accurate balance state [18]. Collision avoidance mainly depends on the repulsive potential [15]. The distribution and shape of the surrounding UAVs and obstacles are reflected as the intensities of the APF functions. According to the intensities, the heading and velocity of the UAV are determined. However, There are two challenges in this field. Firstly, the APF method cares less of the concept of the communication topology and communication weights, resulting in

The associate editor coordinating the review of this manuscript and approving it for publication was Juan Liu.

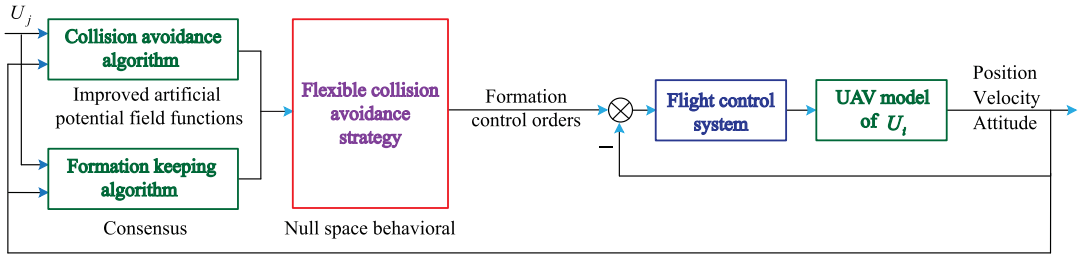

FIGURE 1. Structure of collision avoidance for the formation of multi-UAV.

that the safety of the important members in the formation is hard to be primarily guaranteed. Secondly, most collision avoidance algorithms can not keep a geometric configuration simultaneously, namely, weakly rigid formation [19].

To overcome the first flaw, the consensus approach, which requires only neighbor-to-neighbor interaction and makes full use of the information flow and sharing, provides the heuristic thoughts [20], [21]. In this regard, it is noted that the communication topology of consensus is feasible to reflect the safety priority of each UAV. For example, the UAVs identified as the root nodes can be authorized with high safety priorities, the branch nodes with low safety priorities, and the leaf nodes with the lowest safety priorities. Thus, it is prospective to utilize the communication topology to directly reform the APF function.

Besides, the consensus approach is an effective way to realize formation keeping of multi-UAV. Consensus can make the formation evolve as a rigid body to maintain the predefined geometric relationship and move in a given direction [22]. More precisely, the consensus assures that the UAVs achieve formation keeping in the given velocity, heading, and altitude commands [23].

For solving the second problem, the null space behavioral (NSB) approach is a promising selection [24]. The uniqueness of the NSB approach comes from the way that different tasks are combined into a single motion command [25]. The completion of the high-priority tasks is guaranteed by projecting the low-priority tasks onto the null space of the high-priority ones, and the low-priority tasks are fulfilled if they do not contradict with the high-priority ones [26]. In [27], experimental validation of the NSB approach is provided for formation control. Schlanbush R. and Kristiansen R. try to combine different tasks in the spacecraft formation, where the NSB approach is implemented by giving each task different priorities and then calculating the desired velocity for each spacecraft and each task [28]. Inspired by this, we treat collision avoidance and formation keeping as two different tasks and apply the NSB approach to merging them.

A flexible collision avoidance strategy combining improved APF (IAPF) and consensus is proposed for the formation of multi-UAV in this paper. First, to make full use of the information flow from communication and derive the safety priority of each UAV, the IAPF function is constructed by adding the communication topology and communication weights. Moreover, the oscillation issue [29] is solved by defining a discontinuous range of the IAPF function. The repulsive potential field between the UAV and an obstacle is also constructed, and an auxiliary repulsive potential determined by the relative velocity between them is defined to make the UAV avoid the obstacle more efficiently. For both collision avoidance within the formation and obstacle avoidance, the virtual velocity field is synthesized to formulate the collision avoidance method. Then, comparing the advantages of the IAPF functions in collision avoidance and the consensus method in formation keeping, a flexible collision avoidance strategy considering them both is proposed based on the NSB approach, generating the formation control orders. Thereinto, the formation keeping algorithm is designed as a second-order consensus algorithm.

The main contribution of this work is twofold. Firstly, a novel type of APF function, i.e., the IAPF function, is constructed by adding the communication topology and communication weights, such that the information flow from communication is fully used, and the safety of the important members is primarily assured. Secondly, the proposed collision avoidance strategy can both guarantee collision avoidance and keep a geometric configuration simultaneously, and it is concise in mathematical formulation and easy to implement. In our work, both the IAPF functions and the comprehensive consideration of the collision avoidance and formation keeping problems make the proposed collision avoidance strategy more flexible.

The rest of this paper is organized as follows. First, our proposed structure of the collision avoidance strategy for the formation of multi-UAV is described. Then, the IAPF function for collision avoidance within the formation is constructed by adding the communication topology and communication weights, and the IAPF function for obstacle avoidance is designed. Next, a flexible collision avoidance strategy of the multi-UAV, considering both collision avoidance and formation keeping, is proposed based on the NSB approach. Finally, simulation results with five UAVs are shown that both collision avoidance and formation keeping are realized by the proposed collision avoidance strategy.

II. COLLISION AVOIDANCE ALGORITHM FOR THE FORMATION OF MULTIPLE UNMANNED AERIAL VEHICLES

Figure 1 describes our proposed structure of collision avoidance for the formation of multi-UAV, including four parts,

such as the flight control system, flexible collision avoidance strategy, collision avoidance algorithm based on IAPF, and formation keeping algorithm based on consensus.

The flight control system is aimed at controlling the attitude in the inner-loop, and the collision avoidance strategy is aimed at controlling the position in the outer-loop. The output of the outer-loop is used as the input of the inner-loop. As designing the flight control system is not the focus of this paper, it is omitted here, and more details can be found in our previous publication [30]. The formation control orders, which are generated by the collision avoidance strategy according to the multi-UAV requirements, are given to the flight control system.

The other two parts are the collision avoidance algorithm based on IAPF and the formation keeping algorithm based on consensus. Combining the advantages of IAPF in collision avoidance and consensus in formation keeping, a flexible collision avoidance strategy based on the NSB approach is proposed. The collision avoidance strategy aims at both realizing collision avoidance and keeping a geometric configuration.

III. IMPROVED ARTIFICIAL POTENTIAL FIELD FUNCTIONS

The traditional APF functions ignore the communication topology of the formation. In this situation, it is not coincident with the reality and can not make full use of the information flow from the communication of the formation. Meanwhile, due to the lack of different communication weights, the priority of each UAV is uneasy to derive, and their different importances are unavailable to distinguish.

We add the communication topology and communication weights to the traditional APF functions to overcome the above two flaws, and then a new IAPF function is constructed. Before that, some preliminaries of graph theory are reviewed.

Consider the formation of n identical UAVs, and each UAV is denoted as U_i for $i \in \{1, 2, \cdots, n\}$. All UAVs in the formation constitute a directed graph (digraph) $\mathcal{G} = \{\mathcal{V}, \mathcal{E}\}$, where $\mathcal{V} = \{U_1, U_2, \cdots, U_n\}$ is the set of nodes. $\mathcal{E} = \mathcal{V} \times \mathcal{V}$ is the set of edges, and an edge of the digraph $\mathcal{G}$ is denoted as e_{ij}. e_{ij} is a directed edge from U_j to U_i that U_i can get the information comprised of position, velocity, and attitude from U_j. The set of the neighbors for U_i is denoted as $\mathcal{N}_i = \{U_j \in \mathcal{V} : e_{ij} \in \mathcal{E}\}$. The nonnegative adjacency weight associated with the edge e_{ij} is defined as a_{ij}, and it is assumed that $a_{ii} = 0$ for all $U_i \in \mathcal{V}$. The digraph $\mathcal{G}$ indicates the communication topology of the formation. If the formation can achieve consensus, $\mathcal{G}$ should have a directed spanning tree [31].

The IAPF function between U_i and U_j is represented as $J_{ij}(\|\boldsymbol{\rho}_{ij}\|)$, where $j \in \{1, 2, \cdots, n\}, j \neq i$. $\boldsymbol{\rho}_{ij}$ is the position vector from U_j to U_i, and $\|\cdot\|$ is L_2 norm. $J_{ij}(\|\boldsymbol{\rho}_{ij}\|)$ is determined by the relative distance $\|\boldsymbol{\rho}_{ij}\|$. The schematic drawing of the IAPF functions for the formation composed of three UAVs is depicted in Fig. 2.

The IAPF function of U_i is written as $J_i(\boldsymbol{\rho}_i)$, where $\boldsymbol{\rho}_i$ is the three-dimensional position of U_i. Suppose that $J_i(\boldsymbol{\rho}_i)$ is differentiable for every point in the three-dimensional space.

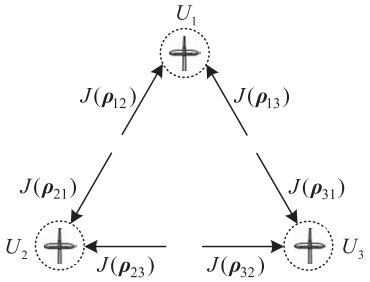

FIGURE 2. Schematic drawing of the improved artificial potential field functions.

$J_i(\boldsymbol{\rho}_i)$ is the sum of the respective IAPF function $J_{ij}(\|\boldsymbol{\rho}_{ij}\|)$, and both $J_i(\boldsymbol{\rho}_i)$ and $J_{ij}(\|\boldsymbol{\rho}_{ij}\|)$ are nonnegative. Then, A UAV can only get the information from the ones who transmit to it [32], and $J_i(\boldsymbol{\rho}_i)$ is defined as

$$J_i(\boldsymbol{\rho}_i) = \sum_{j \in \mathcal{N}_i} a_{ij} J_{ij}(\|\boldsymbol{\rho}_{ij}\|) \tag{1}$$

In Eq. (1), the definition of the IAPF function is different from that of the traditional APF functions that every two UAVs can construct an APF function. Firstly, only when a UAV transmits information to U_i, i.e., $j \in \mathcal{N}_i$, it takes part in the IAPF function of U_i. Secondly, adding a_{ij} means that the UAVs with different communication weights choose different IAPF functions. When U_i maneuvers for collision avoidance, it separates from the UAV with high communication weight primarily. Therefore, the safety priority of collision avoidance is correlated to the communication topology. The UAVs identified as the root nodes have high safety priorities, the branch nodes have low safety priorities, and the leaf nodes have the lowest safety priorities. In other words, if the collision happens within the formation, it is more likely to happen between the UAVs identified as the leaf nodes. In this case, the communication topology of the rest UAVs still has a directed spanning tree, and the formation remains stable. As a result, The IAPF function has good fault tolerance and robustness.

The IAPF function $J_{ij}(\|\boldsymbol{\rho}_{ij}\|)$ between U_i and U_j in Eq. (1) contains an attractive potential and a repulsive potential, and it is expressed as

$$J_{ij}(\|\boldsymbol{\rho}_{ij}\|) = J_{ij}^a(\|\boldsymbol{\rho}_{ij}\|) + J_{ij}^r(\|\boldsymbol{\rho}_{ij}\|) \tag{2}$$

where $J_{ij}^a(\|\boldsymbol{\rho}_{ij}\|)$ and $J_{ij}^r(\|\boldsymbol{\rho}_{ij}\|)$ are the attractive potential and repulsive potential between U_i and U_j, respectively. There exists a unique distance $\|\boldsymbol{\rho}_{ij}^d\|$, where the attractive part and repulsive part balance with each other, and $J_{ij}(\|\boldsymbol{\rho}_{ij}\|)$ has a unique minimum value here. $\boldsymbol{\rho}_{ij}^d$ is the predefined distance between U_i and U_j, and it is also the balanced state of the formation. Furthermore, the gradients of $J_{ij}^a(\|\boldsymbol{\rho}_{ij}\|)$ and $J_{ij}^r(\|\boldsymbol{\rho}_{ij}\|)$ are determined by

$$\begin{cases} \nabla J_{ij}^a(\|\boldsymbol{\rho}_{ij}\|) = \dfrac{\partial J_{ij}^a(\|\boldsymbol{\rho}_{ij}\|)}{\partial \|\boldsymbol{\rho}_{ij}\|} \nabla \boldsymbol{\rho}_{ij} \\ \nabla J_{ij}^r(\|\boldsymbol{\rho}_{ij}\|) = \dfrac{\partial J_{ij}^r(\|\boldsymbol{\rho}_{ij}\|)}{\partial \|\boldsymbol{\rho}_{ij}\|} \nabla \boldsymbol{\rho}_{ij} \end{cases} \tag{3}$$

where $\nabla(\boldsymbol{\rho}_{ij}) = \frac{\boldsymbol{\rho}_i - \boldsymbol{\rho}_j}{\|\boldsymbol{\rho}_{ij}\|}$. Combining Eqs. (1) - (3), the IAPF function is designed to include the communication topology and communication weights.

Collision avoidance can be classified into two types in terms of collision avoidance within the formation and obstacle avoidance. However, there are significant differences between these two situations that the UAVs can avoid each other mutually, while the obstacles can not voluntarily avoid the UAVs. Therefore, different IAPF functions should be constructed to accommodate different situations, which is denoted afterward.

A. IMPROVED ARTIFICIAL POTENTIAL FIELD FUNCTION FOR COLLISION AVOIDANCE WITHIN THE FORMATION

When the distance between the UAVs is smaller than that under normal circumstances, the repulsive part operates primarily in the IAPF function for collision avoidance within the formation. The repulsive part is adopted as an exponential form, and its advantage is that the repulsive potential increases faster and faster as the UAVs get close to each other. Then, the repulsive potential is constructed as a general Morse function [33]

$$J_{ij}^{r}(\|\boldsymbol{\rho}_{ij}\|) = \begin{cases} \dfrac{b}{e^{\frac{\|\boldsymbol{\rho}_{ij}\|}{c}} - e^{\frac{\|\boldsymbol{\rho}_{ij}\|_{\min}}{c}}}, & \|\boldsymbol{\rho}_{ij}\| \in D \\ 0, & \text{otherwise} \end{cases} \tag{4}$$

where b, c are constant parameters, controlling the amplitude and range of the repulsive potential, respectively. The minimum safety distance is defined as $\|\boldsymbol{\rho}_{ij}\|_{\min}$. When the distance between the two UAVs approaches $\|\boldsymbol{\rho}_{ij}\|_{\min}$, the repulsive potential becomes positive infinite.

$$\lim_{\|\boldsymbol{\rho}_{ij}\| \to \|\boldsymbol{\rho}_{ij}\|_{\min}} J_{ij}^{r}(\|\boldsymbol{\rho}_{ij}\|) = +\infty \tag{5}$$

The domain $D = (\|\boldsymbol{\rho}_{ij}\|_{\min}, \ r_1] \cup (r_2, \ \|\boldsymbol{\rho}_{ij}\|_{\max}]$ in Eq. (4) determines the range of the IAPF function for collision avoidance within the formation, and $\|\boldsymbol{\rho}_{ij}\|_{\max}$ is the maximum distance for the IAPF function. If the distance between U_i and U_j exceeds $\|\boldsymbol{\rho}_{ij}\|_{\max}$, the IAPF function does not work at all. When $\|\boldsymbol{\rho}_{ij}\| \le \|\boldsymbol{\rho}_{ij}\|_{\min}$, U_i and U_j crash with each other. As illustrated in Fig. 3, the blue zone depicts the range D of the IAPF function for collision avoidance within the formation.

Why is D a sectionalized domain? Generally, the value of the IAPF function at the balanced state is set to zero; then it is attractive if it is larger than zero, and it is repulsive if it is smaller than zero. In this situation, frequent unstable switch around the balanced state arises. In some literature, it is called the oscillation issue [29]. Hence, the IAPF function set to zero around the balanced state is more beneficial to stability. When $r_1 < \|\boldsymbol{\rho}_{ij}\| \le r_2$, the value of the IAPF function is set to zero. r_1 is the lower bound value around balanced state, and r_2 is the upper bound value. There is a rigorous condition that $\|\boldsymbol{\rho}_{ij}\|_{\min} < r_1 < \|\boldsymbol{\rho}_{ij}^{d}\| < r_2 < \|\boldsymbol{\rho}_{ij}\|_{\max}$. Thus, the range of the IAPF function is defined as

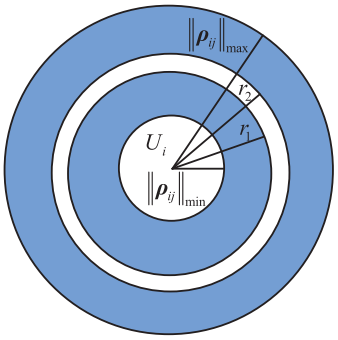

FIGURE 3. Range of the improved artificial potential field function for collision avoidance within the formation.

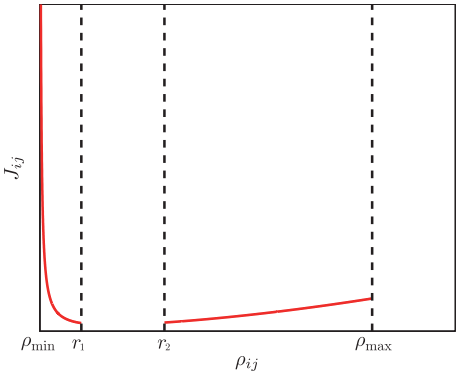

FIGURE 4. Improved artificial potential field function between U_i and U_j.

$D = (\|\boldsymbol{\rho}_{ij}\|_{\min}, \ r_1] \cup (r_2, \ \|\boldsymbol{\rho}_{ij}\|_{\max}]$, which promotes collision avoidance within the formation to work stably. In a word, the reasonable definition of the range of the IAPF function ensures that the oscillation problem is avoided around the balanced state.

Next, the attractive potential is defined as

$$J_{ij}^{a}(\|\boldsymbol{\rho}_{ij}\|) = \begin{cases} \dfrac{1}{2} k_{ij} \|\boldsymbol{\rho}_{ij}\|^2, & \|\boldsymbol{\rho}_{ij}\| \in D \\ 0, & \text{otherwise} \end{cases} \tag{6}$$

where k_{ij} is a positive gain and it determines the intensity of the attractive potential.

Based on Eqs. (4) and (6), the IAPF function between U_i and U_j is obtained for $\|\boldsymbol{\rho}_{ij}\| \in D$ as

$$J_{ij}(\|\boldsymbol{\rho}_{ij}\|) = \frac{1}{2} k_{ij} (\|\boldsymbol{\rho}_{ij}\|)^2 + \frac{b}{e^{\frac{\|\boldsymbol{\rho}_{ij}\|}{c}} - e^{\frac{\|\boldsymbol{\rho}_{ij}\|_{\min}}{c}}} \tag{7}$$

It is obvious that $J_{ij}(\|\boldsymbol{\rho}_{ij}\|) \ge 0$ from Eq. (7). Figure 4 shows the relationship between $J_{ij}(\|\boldsymbol{\rho}_{ij}\|)$ and $\|\boldsymbol{\rho}_{ij}\|$. It can be seen that $\|\boldsymbol{\rho}_{ij}\| \to \|\boldsymbol{\rho}_{ij}\|_{\min}$ as $J_{ij}(\|\boldsymbol{\rho}_{ij}\|) \to +\infty$. The IAPF function is piecewise. Firstly, when $\|\boldsymbol{\rho}_{ij}\| \in (\|\boldsymbol{\rho}_{ij}\|_{\min}, r_1]$, the repulsive potential operates mainly; Secondly, when $\|\boldsymbol{\rho}_{ij}\| \in (r_2, \|\boldsymbol{\rho}_{ij}\|_{\max}]$, the attractive potential operates mainly; Thirdly, when $\|\boldsymbol{\rho}_{ij}\| \in (r_1, r_2] \cup (\|\boldsymbol{\rho}_{ij}\|_{\max}, \infty)$, $J_{ij}(\|\boldsymbol{\rho}_{ij}\|) = 0$.

Invoking Eqs. (2) and (7), the attractive and repulsive potentials are synthesized to get the IAPF function of U_i for $\|\boldsymbol{\rho}_{ij}\| \in D$ as

$$J_i(\boldsymbol{\rho}_i)=\sum_{j\in\mathcal{N}_i}\frac{1}{2}a_{ij}k_{ij}(\|\boldsymbol{\rho}_{ij}\|)^2+\sum_{j\in\mathcal{N}_i}a_{ij}\frac{b}{e^{\frac{\|\boldsymbol{\rho}_{ij}\|}{c}}-e^{\frac{\|\boldsymbol{\rho}_{ij}\|_{\min}}{c}}} \tag{8}$$

After obtaining the IAPF function for collision avoidance within the formation, it is essential to define a virtual velocity potential related to the distances between the UAVs to realize collision avoidance. According to Eqs. (3) and (8), the virtual velocity potential is obtained for collision avoidance within the formation. The virtual velocity potential is written as

$$\begin{aligned}\boldsymbol{V}_i(\boldsymbol{\rho}_i) &= -\nabla J_i(\boldsymbol{\rho}_i)\\ &= -\sum_{j\in\mathcal{N}_i}a_{ij}\nabla J_{ij}^a(\|\boldsymbol{\rho}_{ij}\|)-\sum_{j\in\mathcal{N}_i}a_{ij}\nabla J_{ij}^r(\|\boldsymbol{\rho}_{ij}\|)\\ &= \sum_{j\in\mathcal{N}_i}a_{ij}\Bigg[\frac{b}{c}\cdot\frac{1}{(e^{\frac{\|\boldsymbol{\rho}_{ij}\|}{c}}-e^{\frac{\|\boldsymbol{\rho}_{ij}\|_{\min}}{c}})^2}e^{\frac{\|\boldsymbol{\rho}_{ij}\|}{c}}\\ &\quad -k_{ij}\|\boldsymbol{\rho}_{ij}\|\Bigg]\nabla(\boldsymbol{\rho}_{ij})\end{aligned} \tag{9}$$

Equation (9) takes into account the communication topology and communication weights. Using Eq. (9), once the communication is connected, the multi-UAV could take full advantage of the information flow to realize collision avoidance within the formation. When the formation clusters stably, the IAPF function $J_i(\boldsymbol{\rho}_i)$ achieves the minimum value of zero.

For keeping a rigid configuration, every branch potential in Eq. (9) should be balanced. As $a_{ij} \neq 0$ and $\nabla(\boldsymbol{\rho}_{ij}) \neq 0$, the parameters k_{ij}, b, and c for the balanced state $\|\boldsymbol{\rho}_{ij}^d\|$ should satisfy that

$$\frac{b}{c}\cdot\frac{1}{(e^{\frac{\|\boldsymbol{\rho}_{ij}^d\|}{c}}-e^{\frac{\|\boldsymbol{\rho}_{ij}\|_{\min}}{c}})^2}e^{\frac{\|\boldsymbol{\rho}_{ij}^d\|}{c}}-k_{ij}\|\boldsymbol{\rho}_{ij}^d\|=0 \tag{10}$$

If b, c are given, k_{ij} can be calculated as

$$k_{ij}=\frac{1}{\|\boldsymbol{\rho}_{ij}^d\|}\cdot\frac{b}{c}\cdot\frac{1}{(e^{\frac{\|\boldsymbol{\rho}_{ij}^d\|}{c}}-e^{\frac{\|\boldsymbol{\rho}_{ij}\|_{\min}}{c}})^2}e^{\frac{\|\boldsymbol{\rho}_{ij}^d\|}{c}} \tag{11}$$

B. IMPROVED ARTIFICIAL POTENTIAL FIELD FUNCTION FOR OBSTACLE AVOIDANCE

The IAPF function can also be applied to obstacle avoidance in the airspace. However, there is a significant difference between obstacle avoidance and collision avoidance within the formation that the obstacles can not avoid the UAVs by themselves. Thus, as the distance between a UAV and the obstacle changes, the intensity of the IAPF function should be adjusted more relevantly. Though the obstacles can not voluntarily avoid UAVs, the repulsive potential can be designed more intensive as the multi-UAV gets close to the obstacles. Also, the attractive potential is no longer necessary as the formation does not need getting close to the obstacles.

Suppose that the position of the obstacle is $\boldsymbol{\rho}_o = (x_o, y_o, z_o)^T$. The repulsive potential between U_i and the obstacle is designed as

$$J_i^r(\|\boldsymbol{\rho}_{io}\|)=\begin{cases}[1+k(V_{io})]\cdot\dfrac{b_o}{e^{\frac{\|\boldsymbol{\rho}_{io}\|}{c_o}}-e^{\frac{\|\boldsymbol{\rho}_{io}\|_{\min}}{c_o}}}, & \|\boldsymbol{\rho}_{io}\|\in E\\ 0, & \text{otherwise}\end{cases} \tag{12}$$

and

$$k(V_{io})=\begin{cases}e^{-\frac{1}{V_{io}}}, & V_{io}>0 \quad \text{and} \quad \|\boldsymbol{\rho}_{io}\|\in E\\ 0, & \text{otherwise}\end{cases} \tag{13}$$

where b_o, c_o are constants, controlling the amplitude and range of the repulsive potential, respectively. $E=(\|\boldsymbol{\rho}_{io}\|_{\min}, \|\boldsymbol{\rho}_{io}\|_{\max}]$ determines the range of the repulsive potential $J_i^r(\|\boldsymbol{\rho}_{io}\|)$, where $\|\boldsymbol{\rho}_{io}\|_{\min}$ is the minimum safety distance between U_i and the obstacle, and $\|\boldsymbol{\rho}_{io}\|_{\max}$ is the upper bound value of the range of $J_i^r(\|\boldsymbol{\rho}_{io}\|)$. If the distance between them is larger than $\|\boldsymbol{\rho}_{io}\|_{\max}$, there is no need to avoid the obstacle. V_{io} represents the velocity of the obstacle relative to U_i that $V_{io} > 0$ as the obstacle gets close, $V_{io} < 0$ as the obstacle gets far away, and $V_{io} = 0$ as the obstacle is relatively static. The coefficient $0 < k(V_{io}) < 1$ increases with V_{io}.

The repulsive potential generated by the relative velocity V_{io} in Eq. (13) can be recognized as an auxiliary repulsive potential, which is shown by

$$J_i^r(\|\boldsymbol{\rho}_{io}\|)_{\text{aux}}=k(V_{io})\cdot\frac{b_o}{e^{\frac{\|\boldsymbol{\rho}_{io}\|}{c_o}}-e^{\frac{\|\boldsymbol{\rho}_{io}\|_{\min}}{c_o}}} \tag{14}$$

The auxiliary repulsive potential $J_i^r(\|\boldsymbol{\rho}_{io}\|)_{\text{aux}}$ is introduced to improve the control effort of obstacle avoidance. In other words, it compensates for the weakness that the obstacles can not voluntarily avoid the UAVs.

Let $\nabla(\boldsymbol{\rho}_{io})=\frac{\boldsymbol{\rho}_i-\boldsymbol{\rho}_o}{\|\boldsymbol{\rho}_{io}\|}$, and the virtual velocity potential for obstacle avoidance is obtained as

$$\begin{aligned}\boldsymbol{V}_i(\boldsymbol{\rho}_{io}) &= -\nabla J_i^r(\|\boldsymbol{\rho}_{io}\|)\\ &= (1+e^{-\frac{1}{V_o}})\cdot\frac{b_o}{c_o}\cdot\frac{1}{(e^{\frac{\|\boldsymbol{\rho}_{io}\|}{c_o}}-e^{\frac{\|\boldsymbol{\rho}_{io}\|_{\min}}{c_o}})^2}\\ &\quad\cdot e^{\frac{\|\boldsymbol{\rho}_{io}\|}{c_o}}\nabla(\boldsymbol{\rho}_{io})\end{aligned} \tag{15}$$

So far, both the IAPF function for collision avoidance within the formation and that for obstacle avoidance are constructed, and they are transformed into the virtual velocity potentials as Eqs. (9) and (15). Next, the flexible collision avoidance strategy is proposed based on these IAPF functions.

IV. FLEXIBLE COLLISION AVOIDANCE STRATEGY FOR THE FORMATION OF MULTI-UAV

To enhance the performance of formation control, the flexible collision avoidance strategy comparing the IAPF functions and the consensus method is proposed in the following. Before giving the flexible collision avoidance strategy,

the collision avoidance algorithm based on IAPF and the formation keeping algorithm based on consensus are designed, respectively.

A. COLLISION AVOIDANCE ALGORITHM BASED ON THE IMPROVED ARTIFICIAL POTENTIAL FIELD FUNCTIONS

To design the collision avoidance algorithm, we need comprehensive consideration with the information of the current UAV, the neighbor UAVs, and the obstacles. Combining the virtual velocity potential (9) for collision avoidance within the formation and the virtual velocity potential (15) for obstacle avoidance, if $\|\boldsymbol{\rho}_{ij}\| \in D$ and $\|\boldsymbol{\rho}_{io}\| \in E$, the virtual velocity potential $\boldsymbol{V}_i^t(\boldsymbol{\rho}_i)$ of U_i is obtained as

$$\begin{aligned}\boldsymbol{V}_i^t(\boldsymbol{\rho}_i) &= \boldsymbol{V}_i(\boldsymbol{\rho}_i) + \boldsymbol{V}_i(\boldsymbol{\rho}_{io}) \\ &= \sum_{j\in\mathcal{N}_i} a_{ij}\Bigg[\frac{b}{c}\cdot\frac{1}{(e^{\frac{\|\boldsymbol{\rho}_{ij}\|}{c}} - e^{\frac{\|\boldsymbol{\rho}_{ij}\|_{\min}}{c}})^2} e^{\frac{\|\boldsymbol{\rho}_{ij}\|}{c}} \\ &\quad - k_{ij}\|\boldsymbol{\rho}_{ij}\|\Bigg]\nabla(\boldsymbol{\rho}_{ij}) + (1+e^{-\frac{1}{V_o}})\cdot\frac{b_o}{c_o} \\ &\quad \cdot\frac{1}{(e^{\frac{\|\boldsymbol{\rho}_{io}\|}{c_o}} - e^{\frac{\|\boldsymbol{\rho}_{io}\|_{\min}}{c_o}})^2} e^{\frac{\|\boldsymbol{\rho}_{io}\|}{c_o}}\nabla(\boldsymbol{\rho}_{io}) \end{aligned} \tag{17}$$

By computing the virtual velocity potential, a series of velocity, pitch angle, and heading angle orders are generated to realize collision avoidance and obstacle avoidance. Collision avoidance and obstacle avoidance are actuated by changing the velocity vector of each UAV. Therefore, the desired velocity vector for collision avoidance can be defined as

$$\boldsymbol{V}_i^c = \boldsymbol{V}_i^t(\boldsymbol{\rho}_i) + \boldsymbol{V}_i \tag{18}$$

where $\boldsymbol{V}_i$ is the velocity vector of U_i. When the virtual velocity potential (17) is balanced that $\boldsymbol{V}_i^t(\boldsymbol{\rho}_i) = \boldsymbol{0}$, there exists that $\boldsymbol{V}_i^c = \boldsymbol{V}_i$.

For the sake of giving the formation control orders, the desired velocity vector $\boldsymbol{V}_i^c$ can be firstly divided into three channels in the ground coordinate as (18), as shown at the bottom of this page, where V_{xi}^c, V_{yi}^c, and V_{zi}^c are the components of V_i^c in three channels, and V_{xi}, V_{yi}, and V_{zi} are the components of V_i. x_i, y_i, and z_i are the three components of the position $\boldsymbol{\rho}_i = (x_i,\ y_i,\ z_i)^T$. Subsequently, they are transformed into a series of formation control orders, including the desired velocity V_i^c, pitch angle θ_i^c, and heading angle ψ_i^c, which are given by

$$\begin{cases} V_i^c = \sqrt{(V_{xi}^c)^2 + (V_{yi}^c)^2 + (V_{zi}^c)^2} \\ \theta_i^c = \arctan(\dfrac{V_{zi}^c}{V_{xi}^c}) \\ \psi_i^c = \arctan(\dfrac{V_{yi}^c}{V_{xi}^c}) \end{cases} \tag{19}$$

Equation (19) is the proposed collision avoidance algorithm, which can guarantee collision avoidance within the formation and obstacle avoidance simultaneously. Owing to adding the communication topology and communication weights to our IAPF function, the proposed collision avoidance algorithm is safer and more applicable than the traditional APF methods.

B. FORMATION KEEPING ALGORITHM BASED ON CONSENSUS

The formation keeping algorithm is to ensure the coordination variables to be consistent; therefore, how to choose the coordination variables plays the primary role. The coordination variables contains the position variable and velocity coordination variable. $\boldsymbol{V}_i$ can be directly utilized as the velocity coordination variable, whereas the choice of the position coordination variable is much complicated.

For this purpose, the definition of the position coordination variable is given. It is defined as a reference point $\boldsymbol{\rho}_{iF}$, and the position vector from U_i to its reference point is denoted as $\boldsymbol{\rho}_{iF}^d$.

$$\begin{cases} V_{xi}^c = \displaystyle\sum_{j\in\mathcal{N}_i} a_{ij}\left[-k_{ij}\|\boldsymbol{\rho}_{ij}\| + \frac{b}{c}\cdot\frac{1}{(e^{\frac{\|\boldsymbol{\rho}_{ij}\|}{c}} - e^{\frac{\|\boldsymbol{\rho}_{ij}\|_{\min}}{c}})^2} e^{\frac{\|\boldsymbol{\rho}_{ij}\|}{c}}\right]\frac{x_i - x_j}{\|\boldsymbol{\rho}_{ij}\|} \\ \qquad + (1+e^{-\frac{1}{V_o}})\cdot\frac{b_o}{c_o}\cdot\frac{1}{(e^{\frac{\|\boldsymbol{\rho}_{io}\|}{c_o}} - e^{\frac{\|\boldsymbol{\rho}_{io}\|_{\min}}{c_o}})^2} e^{\frac{\|\boldsymbol{\rho}_{io}\|}{c_o}}\frac{x_i - x_o}{\|\boldsymbol{\rho}_{io}\|} + V_{xi} \\ V_{yi}^c = \displaystyle\sum_{j\in\mathcal{N}_i} a_{ij}\left[-k_{ij}\|\boldsymbol{\rho}_{ij}\| + \frac{b}{c}\cdot\frac{1}{(e^{\frac{\|\boldsymbol{\rho}_{ij}\|}{c}} - e^{\frac{\|\boldsymbol{\rho}_{ij}\|_{\min}}{c}})^2} e^{\frac{\|\boldsymbol{\rho}_{ij}\|}{c}}\right]\frac{y_i - y_j}{\|\boldsymbol{\rho}_{ij}\|} \\ \qquad + (1+e^{-\frac{1}{V_o}})\cdot\frac{b_o}{c_o}\cdot\frac{1}{(e^{\frac{\|\boldsymbol{\rho}_{io}\|}{c_o}} - e^{\frac{\|\boldsymbol{\rho}_{io}\|_{\min}}{c_o}})^2} e^{\frac{\|\boldsymbol{\rho}_{io}\|}{c_o}}\frac{y_i - y_o}{\|\boldsymbol{\rho}_{io}\|} + V_{yi} \\ V_{zi}^c = \displaystyle\sum_{j\in\mathcal{N}_i} a_{ij}\left[-k_{ij}\|\boldsymbol{\rho}_{ij}\| + \frac{b}{c}\cdot\frac{1}{(e^{\frac{\|\boldsymbol{\rho}_{ij}\|}{c}} - e^{\frac{\|\boldsymbol{\rho}_{ij}\|_{\min}}{c}})^2} e^{\frac{\|\boldsymbol{\rho}_{ij}\|}{c}}\right]\frac{z_i - z_j}{\|\boldsymbol{\rho}_{ij}\|} \\ \qquad + (1+e^{-\frac{1}{V_o}})\cdot\frac{b_o}{c_o}\cdot\frac{1}{(e^{\frac{\|\boldsymbol{\rho}_{io}\|}{c_o}} - e^{\frac{\|\boldsymbol{\rho}_{io}\|_{\min}}{c_o}})^2} e^{\frac{\|\boldsymbol{\rho}_{io}\|}{c_o}}\frac{z_i - z_o}{\|\boldsymbol{\rho}_{io}\|} + V_{zi} \end{cases} \tag{18}$$

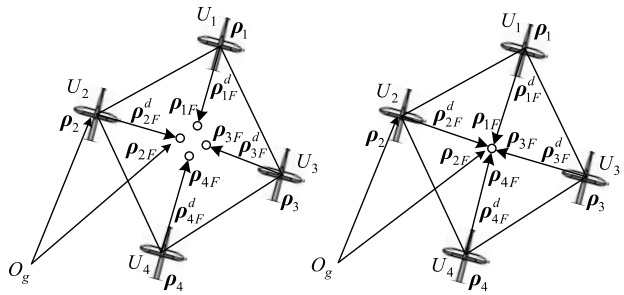

(a) Unsteady case (b) Steady case

FIGURE 5. Position coordination variable ρ_{iF} generated by U_i.

The geometric configuration and position coordination variables for four UAVs are illustrated in Fig. 5 for both the unsteady case and the steady case, where the position coordination variables as represented as small circles. For brevity and clarity, we only mark the position coordination variable $\boldsymbol{\rho}_{2F}$.

It is assumed that the predefined geometric configuration of the formation is known. The position coordination variable is obtained by vector computation

$$\boldsymbol{\rho}_{iF} = \boldsymbol{\rho}_i + \boldsymbol{\rho}^d_{iF} \tag{20}$$

where $\boldsymbol{\rho}^d_{iF}$ is the desired position vector from U_i to its reference point and denotes the geometric constraint of the formation. If $\lim_{t\to\infty} \boldsymbol{\rho}_{iF} \to \boldsymbol{\rho}_{jF}$, formation keeping is achieved as Fig. 5(b). We define the geometric constraint between U_i and U_j as $\boldsymbol{\rho}^d_{ij}$, which is coincident with the description of $\boldsymbol{\rho}^d_{iF}$ and $\boldsymbol{\rho}^d_{jF}$, subject to

$$\begin{aligned}\boldsymbol{\rho}^d_{ij} &= \lim_{\boldsymbol{\rho}_{iF}\to\boldsymbol{\rho}_{jF}} (\boldsymbol{\rho}_i - \boldsymbol{\rho}_j) \\ &= \lim_{\boldsymbol{\rho}_{iF}\to\boldsymbol{\rho}_{jF}} \left[(\boldsymbol{\rho}_{iF} - \boldsymbol{\rho}^d_{iF}) - (\boldsymbol{\rho}_{jF} - \boldsymbol{\rho}^d_{jF})\right] \\ &= \boldsymbol{\rho}^d_{jF} - \boldsymbol{\rho}^d_{iF}\end{aligned} \tag{21}$$

It can be seen that the objective of the consensus method is to make the distances between the UAVs achieve $\boldsymbol{\rho}^d_{ij}$, while the IAPF functions are to make the distances toward $\left\|\boldsymbol{\rho}^d_{ij}\right\|$. That is the reason why the consensus method can keep a geometric formation configuration, but the IAPF functions can not.

Next, a second-order consensus algorithm is adopted to keep the geometric formation configuration. The longitudinal, lateral, and altitudinal channels are designed, respectively, as

$$\begin{cases} \dot{V}^f_{xi} = -\sum_{j\in\mathcal{N}_i} a_{ij}[x_{iF} - x_{jF} + \gamma(V_{xi} - V_{xj})] \\ \dot{V}^f_{yi} = -\sum_{j\in\mathcal{N}_i} a_{ij}[y_{iF} - y_{jF} + \gamma(V_{yi} - V_{yj})] \\ \dot{V}^f_{zi} = -\sum_{j\in\mathcal{N}_i} a_{ij}[z_{iF} - z_{jF} + \gamma(V_{zi} - V_{zj})] \end{cases} \tag{22}$$

where $\dot{V}^f_{xi}$, $\dot{V}^f_{yi}$, and $\dot{V}^f_{zi}$ are the desired longitudinal, lateral, and altitudinal accelerations, respectively. x_{iF}, y_{iF}, and z_{iF} are the three components of the reference point position $\boldsymbol{\rho}_{iF} = (x_{iF},\ y_{iF},\ z_{iF})^T$. γ is a constant and $\gamma > 1$.

Though $\boldsymbol{\rho}_{iF}$ is different from each other in the beginning, the formation is stable if $\lim_{t\to\infty} \boldsymbol{\rho}_{iF} \to \boldsymbol{\rho}_{jF}$ by controlling the accelerations $\dot{V}^f_{xi}$, $\dot{V}^f_{yi}$, and $\dot{V}^f_{zi}$. Then, utilizing the second-order consensus algorithm (22), formation keeping can be achieved. To further design the formation keeping algorithm based on consensus, the desired accelerations $\dot{V}^f_{xi}$, $\dot{V}^f_{yi}$, and $\dot{V}^f_{zi}$ in Eq. (22) are transformed into a set of formation keeping orders as follows:

$$\begin{cases} \dot{V}^f_i = \sqrt{(\dot{V}^f_{xi})^2 + (\dot{V}^f_{yi})^2 + (\dot{V}^f_{zi})^2} \\ \dot{\theta}^f_i = \dfrac{\mathrm{d}}{\mathrm{d}t}[\arctan(\dfrac{V^f_{zi}}{V^f_{xi}})] = \dfrac{\dot{V}^f_{zi}\int_0^t \dot{V}^f_{xi}\mathrm{d}t - \dot{V}^f_{xi}\int_0^t \dot{V}^f_{zi}\mathrm{d}t}{\left(\int_0^t \dot{V}^f_{xi}\mathrm{d}t\right)^2 + \left(\int_0^t \dot{V}^f_{zi}\mathrm{d}t\right)^2} \\ \dot{\psi}^f_i = \dfrac{\mathrm{d}}{\mathrm{d}t}[\arctan(\dfrac{V^f_{yi}}{V^f_{xi}})] = \dfrac{\dot{V}^f_{yi}\int_0^t \dot{V}^f_{xi}\mathrm{d}t - \dot{V}^f_{xi}\int_0^t \dot{V}^f_{yi}\mathrm{d}t}{\left(\int_0^t \dot{V}^f_{xi}\mathrm{d}t\right)^2 + \left(\int_0^t \dot{V}^f_{yi}\mathrm{d}t\right)^2} \end{cases} \tag{23}$$

where $\dot{V}^f_i$, $\dot{\theta}^f_i$, and $\dot{\psi}^f_i$ are the desired acceleration, pitch angle rate, and heading angle rate for formation keeping, respectively.

C. FLEXIBLE COLLISION AVOIDANCE STRATEGY

Combining the advantages of the IAPF functions in collision avoidance and the consensus method in formation keeping, a flexible collision avoidance strategy considering them both is proposed. The proposed collision avoidance strategy can both realize collision avoidance quickly and keep a geometric configuration. Meanwhile, the collision avoidance strategy should take care of processing the conflicts between the two individual algorithms. For example, when the obstacles are in the front, the consensus method attempts to make the multi-UAV fly straightly, while the IAPF functions want the formation to get away from the obstacles. Then, some typical conflicts arise, and how to conquer these conflicts is very important.

The NSB method is good at processing conflict tasks, which is put forward by F. Arrichiello [34]. The null space is the dimensional space not used for performing tasks. For example, the velocity vector of a UAV can be treated as the null space. When the mission is composed of different tasks, the overall velocity is elaborated by properly merging the output of each task. In particular, the velocity of each task is computed if it acts alone. Then, a low-priority task is projected onto the null space of the high-priority task to remove those velocity components which conflict with it.

Collision avoidance and formation keeping can be treated as two different tasks. Collision avoidance has high priority because it has far more to do with flight safety. When formation keeping interferes collision avoidance, it executes weakly and even stops. When they have no conflict, formation keeping operates well with collision avoidance. By projecting

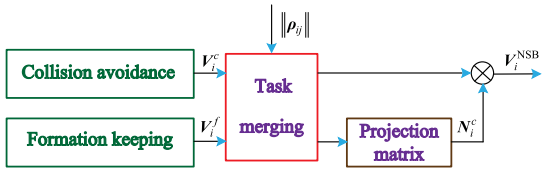

FIGURE 6. Structure of the flexible collision avoidance strategy.

formation keeping with low priority onto collision avoidance, the flexible collision avoidance strategy is designed, where the distance $\|\boldsymbol{\rho}_{ij}\|$ is the dominant factor. The structure of the flexible collision avoidance strategy is shown as Fig. 6.

Combining collision avoidance and formation keeping, the NSB approach has a single output in terms of the NSB velocity order

$$\boldsymbol{V}_i^{\mathrm{NSB}} = \boldsymbol{V}_i^c + \boldsymbol{N}_i^c \boldsymbol{V}_i^f \tag{24}$$

where $\boldsymbol{N}_i^c = (\mathbf{I} - \boldsymbol{P}_i^{c^*} \boldsymbol{P}_i^c)$ is the projection matrix for the null space of the Jacobian determinant $\boldsymbol{P}_i^c$. The definition of $\boldsymbol{P}_i^c$ is given afterward.

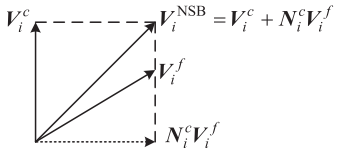

FIGURE 7. NSB vector of the flexible collision avoidance strategy.

Figure 7 depicts the NSB vector of the proposed collision avoidance strategy. $\boldsymbol{V}_i^c$ and $\boldsymbol{V}_i^f$ are the velocity vectors of collision avoidance and formation keeping, respectively. $\boldsymbol{V}_i^f$ has low priority, so it is projected onto the null space of $\boldsymbol{V}_i^c$. In this process, its component conflicting with $\boldsymbol{V}_i^c$ is removed, and the rest is incorporated into $\boldsymbol{V}_i^c$. The compatibility of these two tasks is equivalent to the orthogonality of them.

Let

$$\boldsymbol{V}_i^f = [V_i^f \cos\theta_i^f \cos\psi_i^f,\ V_i^f \cos\theta_i^f \sin\psi_i^f,\ V_i^f \sin\theta_i^f]^T \tag{25}$$

$$\boldsymbol{V}_i^c = [V_i^c \cos\theta_i^c \cos\psi_i^c,\ V_i^c \cos\theta_i^c \sin\psi_i^c,\ V_i^c \sin\theta_i^c]^T \tag{26}$$

The cost function is defined as

$$\begin{aligned}\delta_i^c &= \sum_{j\in\mathcal{N}_i} a_{ij} \|\boldsymbol{\rho}_{ij}\| \\ &= \sum_{j\in\mathcal{N}_i} a_{ij} \sqrt{(x_i - x_j)^2 + (y_i - y_j)^2 + (z_i - z_j)^2}\end{aligned} \tag{27}$$

Then

$$\begin{aligned}\boldsymbol{P}_i^c &= \left(\frac{\partial \delta_i^c}{\partial x_i},\ \frac{\partial \delta_i^c}{\partial y_i},\ \frac{\partial \delta_i^c}{\partial z_i}\right) \\ &= \left(\sum_{j\in\mathcal{N}_i} a_{ij} \frac{x_i - x_j}{\|\boldsymbol{\rho}_{ij}\|}, \sum_{j\in\mathcal{N}_i} a_{ij} \frac{y_i - y_j}{\|\boldsymbol{\rho}_{ij}\|}, \sum_{j\in\mathcal{N}_i} a_{ij} \frac{z_i - z_j}{\|\boldsymbol{\rho}_{ij}\|}\right)\end{aligned} \tag{28}$$

and

$$\dot{\delta}_i^c = \frac{\partial \delta_i^c}{\partial \boldsymbol{\rho}_i} \boldsymbol{V}_i = \boldsymbol{P}_i^c \boldsymbol{V}_i \tag{29}$$

Let $\boldsymbol{V}_i^*$ be the least square solution of $\boldsymbol{V}_i$, and there exists that

$$\boldsymbol{V}_i^* = \boldsymbol{P}_i^{c^*} \dot{\delta}_i^c = \boldsymbol{P}_i^{c^T} (\boldsymbol{P}_i^c \boldsymbol{P}_i^{c^T})^{-1} \dot{\delta}_i^c \tag{30}$$

Comparing with Eq. (24), one has (31), as shown at the bottom of this page.

So far, the NSB velocity vector is obtained. It can also be rewritten into the vector form $\boldsymbol{V}_i^{\mathrm{NSB}} = [V_{xi}^{\mathrm{NSB}}, V_{yi}^{\mathrm{NSB}}, V_{zi}^{\mathrm{NSB}}]^T$. The final formation control orders V_i^{NSB},

$$\begin{aligned}\boldsymbol{V}_i^{\mathrm{NSB}} &= \boldsymbol{V}_i^c + [\mathbf{I} - \boldsymbol{P}_i^{c^*} \boldsymbol{P}_i^c] \boldsymbol{V}_i^f \\ &= \boldsymbol{V}_i^c + \left\{ \mathbf{I} - \begin{bmatrix} \sum_{j\in\mathcal{N}_i} a_{ij} \frac{x_i - x_j}{\|\boldsymbol{\rho}_{ij}\|} \\ \sum_{j\in\mathcal{N}_i} a_{ij} \frac{y_i - y_j}{\|\boldsymbol{\rho}_{ij}\|} \\ \sum_{j\in\mathcal{N}_i} a_{ij} \frac{z_i - z_j}{\|\boldsymbol{\rho}_{ij}\|} \end{bmatrix} \left[\sum_{j\in\mathcal{N}_i} a_{ij} \frac{x_i - x_j}{\|\boldsymbol{\rho}_{ij}\|}, \sum_{j\in\mathcal{N}_i} a_{ij} \frac{y_i - y_j}{\|\boldsymbol{\rho}_{ij}\|} V_i^f, \sum_{j\in\mathcal{N}_i} a_{ij} \frac{z_i - z_j}{\|\boldsymbol{\rho}_{ij}\|} \right] \right\} \boldsymbol{V}_i^f \\ &= \boldsymbol{V}_i^c + \begin{bmatrix} 1 - (\sum_{j\in\mathcal{N}_i} a_{ij} \frac{x_i - x_j}{\|\boldsymbol{\rho}_{ij}\|})^2 & \sum_{j\in\mathcal{N}_i} a_{ij} \frac{x_i - x_j}{\|\boldsymbol{\rho}_{ij}\|} \cdot \sum_{j\in\mathcal{N}_i} a_{ij} \frac{y_i - y_j}{\|\boldsymbol{\rho}_{ij}\|} & \sum_{j\in\mathcal{N}_i} a_{ij} \frac{x_i - x_j}{\|\boldsymbol{\rho}_{ij}\|} \cdot \sum_{j\in\mathcal{N}_i} a_{ij} \frac{z_i - z_j}{\|\boldsymbol{\rho}_{ij}\|} \\ \sum_{j\in\mathcal{N}_i} a_{ij} \frac{x_i - x_j}{\|\boldsymbol{\rho}_{ij}\|} \cdot \sum_{j\in\mathcal{N}_i} a_{ij} \frac{y_i - y_j}{\|\boldsymbol{\rho}_{ij}\|} & 1 - (\sum_{j\in\mathcal{N}_i} a_{ij} \frac{y_i - y_j}{\|\boldsymbol{\rho}_{ij}\|})^2 & \sum_{j\in\mathcal{N}_i} a_{ij} \frac{y_i - y_j}{\|\boldsymbol{\rho}_{ij}\|} \cdot \sum_{j\in\mathcal{N}_i} a_{ij} \frac{z_i - z_j}{\|\boldsymbol{\rho}_{ij}\|} \\ \sum_{j\in\mathcal{N}_i} a_{ij} \frac{x_i - x_j}{\|\boldsymbol{\rho}_{ij}\|} \cdot \sum_{j\in\mathcal{N}_i} a_{ij} \frac{z_i - z_j}{\|\boldsymbol{\rho}_{ij}\|} & \sum_{j\in\mathcal{N}_i} a_{ij} \frac{y_i - y_j}{\|\boldsymbol{\rho}_{ij}\|} \cdot \sum_{j\in\mathcal{N}_i} a_{ij} \frac{z_i - z_j}{\|\boldsymbol{\rho}_{ij}\|} & 1 - (\sum_{j\in\mathcal{N}_i} a_{ij} \frac{z_i - z_j}{\|\boldsymbol{\rho}_{ij}\|})^2 \end{bmatrix} \boldsymbol{V}_i^f \end{aligned} \tag{31}$$

θ^{NSB}, and ψ^{NSB} are given by

$$\begin{cases} V_i^{\mathrm{NSB}} = \sqrt{(V_{xi}^{\mathrm{NSB}})^2 + (V_{yi}^{\mathrm{NSB}})^2 + (V_{zi}^{\mathrm{NSB}})^2} \\ \theta_i^{\mathrm{NSB}} = \arctan(\dfrac{V_{zi}^{\mathrm{NSB}}}{V_{xi}^{\mathrm{NSB}}}) \\ \psi_i^{\mathrm{NSB}} = \arctan(\dfrac{V_{yi}^{\mathrm{NSB}}}{V_{xi}^{\mathrm{NSB}}}) \end{cases} \tag{32}$$

As a result, Eq. (32) is the flexible collision avoidance strategy, which can handle the relationship between collision avoidance and formation keeping flexibly. Utilizing the flexible collision avoidance strategy, the formation of multi-UAV both realizes collision avoidance quickly and keeps a geometric configuration. Besides, Eq. (32) is concise in mathematical formulation and easy to implement.

Finally, as illustrated in Fig. 1, the formation control orders in Eq. (32) are transmitted to the flight control system to follow them. A sophisticated flight control system based on state feedback has been designed for controlling the 6-DOF dynamic UAV in our previous study, which is utilized to correspond to the formation control orders in this paper. Please refer to our previous publication [30] for more details.

V. NUMERICAL SIMULATION

Simulations are performed with Matlab/Simulink, where five identical UAVs are utilized for verifying our collision avoidance strategy. Each UAV weights 85 kg with a wingspan of 2 m, and the definition of the parameters of the 6-DOF dynamic UAV model is given in [30]. Figure 8 shows the communication topology of the formation. The edge from U_j to U_i means that U_i can receive the information comprised of position, velocity, and attitude from U_j.

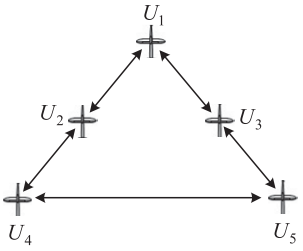

FIGURE 8. Communication topology of the formation of multi-UAV.

All the UAVs have to maintain an equilateral triangular formation with side length of 8 m. Besides, they are not arranged to fly at identical altitude: U_2 and U_3 are desired to maneuver 4 m lower than U_1, while U_4 and U_5 are desired to maneuver 8 m lower than U_1. Concerning the wingspan, this is a tight formation situation available to verify our collision avoidance strategy.

The parameters in Eqs. (4) and (6) are given by $\|\boldsymbol{\rho}_{ij}\|_{\min} = 2$ m, $r_1 = 3.5$ m, $r_2 = 4.5$ m, $\|\boldsymbol{\rho}_{ij}\|_{\max} = 10$ m, $\|\boldsymbol{\rho}_{io}\|_{\min} = 2$ m, and $\|\boldsymbol{\rho}_{io}\|_{\max} = 1000$ m, $\forall j \in \mathcal{N}_i$. The parameters for the virtual velocity potential (17) are chosen as $k_{ij} = 0.0061$, $b = 1, c = 1, b_o = 0.1$, and $c_o = 0.1$. The maximum velocity of the formation is 46 m/s and the minimum is 32 m/s. The initial velocity, pitch angle, and heading angle of the formation are 39 m/s, 0^{o}, and 45^{o}, respectively. The initial positions of each UAV are $\boldsymbol{\rho}_1(t_0) = [1037.5, 1033.4, 999]^T$ m, $\boldsymbol{\rho}_2(t_0) = [1035.6, 1032.9, 997]^T$ m, $\boldsymbol{\rho}_3(t_0) = [1037, 1031.5, 997]^T$ m, $\boldsymbol{\rho}_4(t_0) = [1034.9, 1032.2, 995]^T$ m, and $\boldsymbol{\rho}_5(t_0) = [1036.3, 1030.8, 995]^T$ m, respectively, where t_0 is the initial simulation instant.

The initial simulation parameters mentioned above are with small distances between the UAVs. The distance between U_2 and U_3 is 2 m, which is equivalent to the minimum safety distance $\|\boldsymbol{\rho}_{ij}\|_{\min}$, $\forall j \in \mathcal{N}_i$. In this situation, U_2 and U_3 need to separate from each other urgently. The distance between U_1 and U_2, the distance between U_1 and U_3, the distance between U_2 and U_4, and the distance between U_3 and U_5 are all just 2.8 m that the formation needs to implement collision avoidance immediately.

Different communication weights are set to build different safety priorities for each UAV that $a_{12} = 1.5$, $a_{13} = 1.5$, $a_{21} = 2$, $a_{24} = 1$, $a_{31} = 2$, $a_{35} = 1$, $a_{42} = 1.5$, $a_{45} = 1$, $a_{53} = 1.5$, and $a_{54} = 1$. Thereinto, U_1 has the highest safety priority that it possesses the largest communication weight value of 2. The safety priorities of U_2 and U_3 are inferior to U_1, and their communication weight value is the median of 1.5. Finally, U_4 and U_5 have the lowest safety priorities with the smallest communication weight value of 1. In the simulation, we will show that the safety of the important members as U_1 is primarily guaranteed, followed by that of U_2 and U_3, with the safety of U_2 and U_3 least guaranteed.

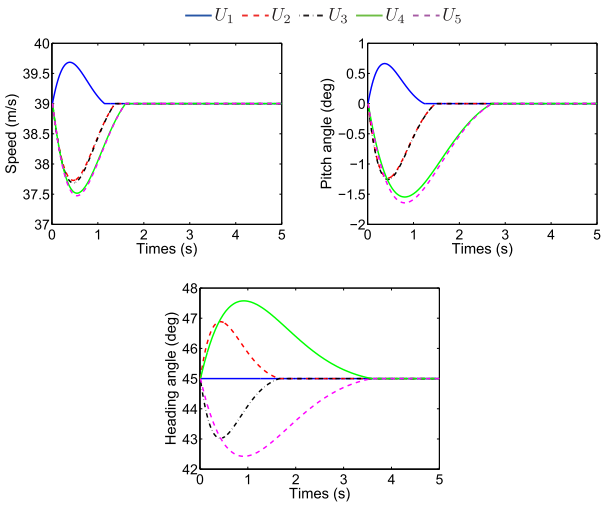

FIGURE 9. Attitudes of collision avoidance within the formation.

The operation step is 0.02 s, and the simulation time is 800 s. Simulations are performed to validate the flexible collision avoidance strategy (32). Figures 9 and 10 describe the velocity, pitch angle, heading angle, planar separation, and altitudinal separation for collision avoidance within the formation. Figures 11, 12, and 13 show the long-time response process of the formation for collision avoidance, especially for obstacle avoidance. In Fig. 14, a comparative

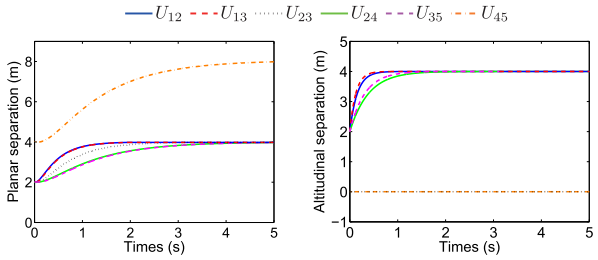

FIGURE 10. Positions of collision avoidance within the formation.

simulation, including planar position, altitudinal position, and three-dimensional trajectory, is performed to show the superior effectiveness of the collision avoidance algorithm with the auxiliary repulsive potential to the algorithm without that.

As shown in Figs. 9 and 10, to manifest the response process of collision avoidance within the formation, only the first 5 s of the simulation result is chosen. It can be seen that only 4.8 s is used before the distances between the UAVs turn normal. The regulation of velocities, pitch angles, and heading angles for U_2 and U_3 are more intensive than that for U_1, meaning that U_1 has higher safety priority and its safety is primarily guaranteed. Similarly, U_2 and U_3 have higher safety priorities than U_4 and U_5, such that the regulation of velocities, pitch angles, and heading angles for U_4 and U_5 are more intensive than that for U_2 and U_3. In addition, the planar separation indicates that the distance between U_1 and U_2 and the distance between U_1 and U_3 get normal with the fastest speed, and then the distance between U_2 and U_3 gets normal, followed by the distance between U_2 and U_4 and the distance between U_3 and U_5, with the distance between U_4 and U_5 getting normal at last. Thus, the simulation result validates the effectiveness and rapidity of our collision avoidance strategy (32), which is good at collision avoidance within the formation and can primarily guarantee the safety of the important members in the formation by adding different communication weights.

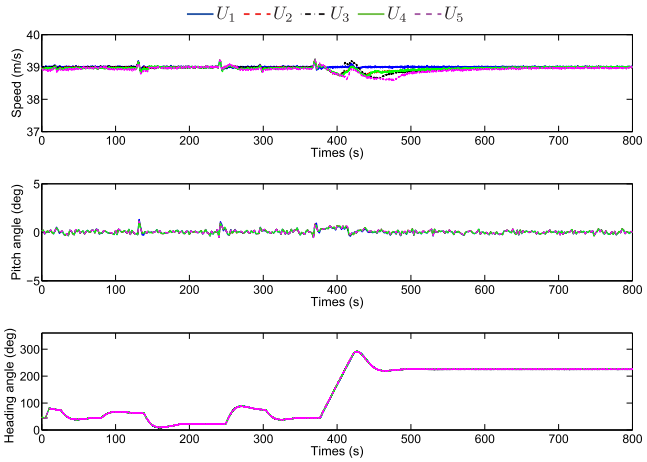

FIGURE 11. Attitudes of the multi-UAV.

Figures 11, 12, and 13 show the long-time simulation results under the flexible collision avoidance strategy (32). The obstacles, which are described as spheres, are localized

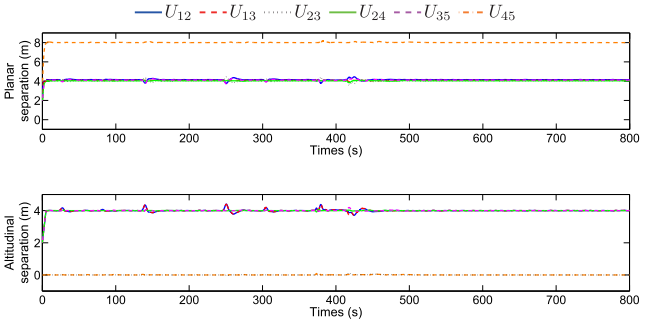

FIGURE 12. Positions of the multi-UAV.

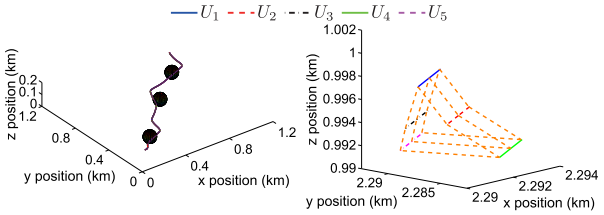

FIGURE 13. Three-dimensional trajectory of the multi-UAV.

on the predefined flight path. By regulating the velocity, pitch angle, and heading angle, the real-time flight path is reasonably adjusted, and the formation gets away from the obstacles successfully and quickly. In the last subfigure of Fig. 13, the local three-dimensional trajectory, where only the last several sampling points are adopted within 0.2 s, is the last part of the whole trajectory. It is worthwhile noticing that the five UAVs maintain a good triangular configuration as desired. Therefore, the simulation result illustrates that our collision avoidance strategy can guarantee a good geometric configuration as well as collision avoidance.

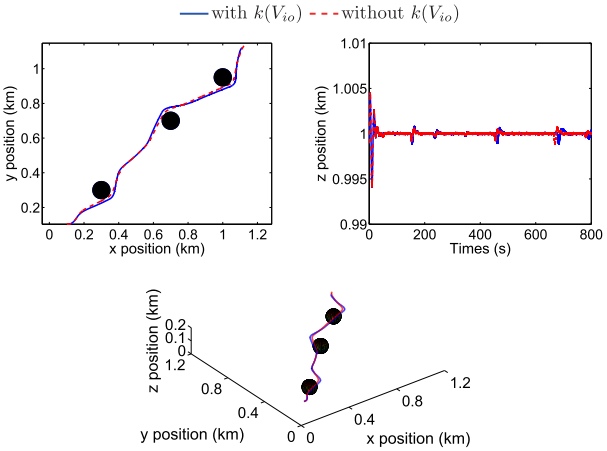

FIGURE 14. Comparison of the collision avoidance algorithms with and without the auxiliary repulsive potential.

Figure 14 provides a comparative simulation for the collision avoidance algorithms with and without the auxiliary repulsive potential in terms of $J_i^r(\|\boldsymbol{\rho}_{io}\|)_{\text{aux}}$ in Eq. (14). It can be seen that the collision avoidance algorithm with

the auxiliary repulsive potential, which is determined by the relative velocity between the UAV and the obstacle, carries out obstacle avoidance earlier and more intensively, so it leads to larger minimum distances away from the obstacles. In other words, the collision avoidance algorithm with the auxiliary repulsive potential outperforms the algorithm without that. Thus, it is concluded that the auxiliary repulsive potential, which assists in improving the control effort of obstacle avoidance, can compensate for the weakness that the obstacles can not avoid the UAVs voluntarily.

VI. CONCLUSION

A flexible collision avoidance strategy based on IAPF and consensus is proposed for the multi-UAV in this paper. By utilizing the communication topology and communication weights to reform the APF function, the information flow from communication is fully used, and the safety of the important members is primarily guaranteed. The proposed strategy is not only good at collision avoidance within the formation, but also avoiding the obstacles outside the formation. By introducing the auxiliary repulsive potential determined by the relative velocity between the UAV and the obstacle, the multi-UAV performs obstacle avoidance more efficiently. In our work, the NSB approach is designed to merge collision avoidance and formation keeping. Both the IAPF functions and the comprehensive consideration of collision avoidance and formation keeping problems make the proposed collision avoidance strategy more flexible. Our proposed collision avoidance strategy is concise in mathematical formulation and easy to implement. Three-dimensional flight simulation with five 6-DOF UAVs indicates that the flexible collision avoidance strategy can both implement collision avoidance quickly and keep a good geometric formation configuration simultaneously.

REFERENCES

[1] M. Brodecki and K. Subbarao, "Autonomous formation flight control system using in-flight sweet-spot estimation," *J. Guid. Control Dyn.*, vol. 38, no. 6, pp. 1083–1096, Jun. 2015.

[2] R. Linares, J. L. Crassidis, and Y. Cheng, "Constrained relative attitude determination for two-vehicle formations," *J. Guid., Control, Dyn.*, vol. 34, no. 2, pp. 1438–1447, 2011.

[3] A. Nemati and M. Kumar, "Control of microcoaxial helicopter based on a reduced-order observer," *J. Aerosp. Eng.*, vol. 29, no. 3, pp. 1–8, 2015.

[4] I. Exarchos, P. Tsiotras, and M. Pachter, "UAV collision avoidance based on the solution of the suicidal pedestrian differential game," in *Proc. AIAA Guid., Navigat., Control Conf.* San Diego, CA, USA: AIAA, Jan. 2016, pp. 1–16.

[5] L. Schmitt and W. Fichter, "Collision-avoidance framework for small fixed-wing unmanned aerial vehicles," *J. Guid., Control, Dyn.*, vol. 37, no. 4, pp. 1323–1329, 2014.

[6] J. Tang, M. A. Piera, and T. Guasch, "Coloured Petri net-based traffic collision avoidance system encounter model for the analysis of potential induced collisions," *Transp. Res. C, Emerg. Technol.*, vol. 67, pp. 357–377, Jun. 2016.

[7] J. Tang, F. Zhu, and M. A. Piera, "A causal encounter model of traffic collision avoidance system operations for safety assessment and advisory optimization in high-density airspace," *Transp. Res. C, Emerg. Technol.*, vol. 96, pp. 347–365, Nov. 2018.

[8] A. Mcfadyen and L. Mejias, "A survey of autonomous vision-based see and avoid for unmanned aircraft systems," *Progr. Aerosp. Sci.*, vol. 80, pp. 1–17, Jan. 2016.

[9] F. Liao, R. Teo, J. L. Wang, X. Dong, F. Lin, and K. Peng, "Distributed formation and reconfiguration control of VTOL UAVs," *IEEE Trans. Control Syst. Technol.*, vol. 25, no. 1, pp. 270–277, Jan. 2017.

[10] C. Hanses, "On airborne collision avoidance system's compatibility with segmented independent parallel approach procedures," *J. Aircr.*, vol. 52, no. 3, pp. 956–963, 2015.

[11] Y. I. Jenie, E.-J. van Kampen, C. C. de Visser, J. Ellerbroek, and J. M. Hoekstra, "Selective velocity obstacle method for deconflicting maneuvers applied to unmanned aerial vehicles," *J. Guid., Control, Dyn.*, vol. 38, no. 6, pp. 1–6, 2015.

[12] N. E. Smith, R. G. Cobb, S. J. Pierce, and V. M. Raska, "Uncertainty corridors for three-dimensional collision avoidance," *J. Guid., Control, Dyn.*, vol. 30, no. 12, pp. 1–7, 2015.

[13] Y.-B. Chen, G.-C. Luo, Y.-S. Mei, J.-Q. Yu, and X.-L. Su, "UAV path planning using artificial potential field method updated by optimal control theory," *Int. J. Syst. Sci.*, vol. 47, no. 6, pp. 1407–1420, 2014.

[14] J. Seo, Y. Kim, S. Kim, and A. Tsourdos, "Collision avoidance strategies for unmanned aerial vehicles in formation flight," *IEEE Trans. Aerosp. Electron. Syst.*, vol. 53, no. 6, pp. 2718–2734, Dec. 2017.

[15] O. Cetin and G. Yilmaz, "Real-time autonomous UAV formation flight with collision and obstacle avoidance in unknown environment," *J. Intell. Robot. Syst.*, vol. 42, nos. 1–4, pp. 415–433, 2016.

[16] J.-D. Seong and H.-D. Kim, "Multiobjective optimization for collision avoidance maneuver using a genetic algorithm," *Proc. Inst. Mech. Eng., G, J. Aerosp. Eng.*, vol. 230, no. 8, pp. 1438–1447, 2015.

[17] L. Zhu, X. Cheng, and F. G. Yuan, "A 3D collision avoidance strategy for UAV with physical constraints," *Measurement*, vol. 77, pp. 40–49, Jan. 2016.

[18] O. Khatib, "Real-time obstacle avoidance for manipulators and mobile robots," *Int. J. Robot. Res.*, vol. 5, no. 1, pp. 90–98, 1986.

[19] M. Radmanesh and M. Kumar, "Flight formation of UAVs in presence of moving obstacles using fast-dynamic mixed integer linear programming," *Aerosp. Sci. Technol.*, vol. 50, pp. 149–160, Mar. 2016.

[20] A. Abdessameud and A. Tayebi, "Formation control of VTOL unmanned aerial vehicles with communication delays," *Automatica*, vol. 47, no. 11, pp. 2383–2394, Nov. 2011.

[21] Y. Liu, J. M. Montenbruck, D. Zelazo, M. Odelga, S. Rajappa, H. H. Bülthoff, F. Allgöwer, and A. Zell, "A distributed control approach to formation balancing and maneuvering of multiple multirotor UAVs," *IEEE Trans. Robot.*, vol. 34, no. 4, pp. 870–882, Aug. 2018.

[22] H. M. Guzey, "Hybrid consensus-based formation control of fixed-wing MUAVs," *Cybern. Syst.*, vol. 48, no. 2, pp. 71–83, 2017.

[23] M. Kabiri, H. Atrianfar, and M. B. Menhaj, "Formation control of VTOL UAV vehicles under switching-directed interaction topologies with disturbance rejection," *Int. J. Control*, vol. 91, no. 1, pp. 33–44, 2018.

[24] G. Antonelli, E. Arrichiello, and S. Chiaverini, "Experiments of formation control with multirobot systems using the null-space-based behavioral control," *IEEE Trans. Control Syst. Technol.*, vol. 17, no. 5, pp. 1173–1182, Sep. 2009.

[25] N. R. Gans, G. Q. Hu, K. Nagarajan, and W. E. Dixon, "Keeping multiple moving targets in the field of view of a mobile camera," *IEEE Trans. Robot.*, vol. 27, no. 4, pp. 822–828, Aug. 2011.

[26] A. Marino, L. E. Parker, G. Antonelli, and F. Caccavale, "A decentralized architecture for multi-robot systems based on the null-space-behavioral control with application to multi-robot border patrolling," *J. Intell. Robot. Syst.*, vol. 71, nos. 3–4, pp. 423–444, 2013.

[27] G. Antonelli, "Stability analysis for prioritized closed-loop inverse kinematic algorithms for redundant robotic systems," *IEEE Trans. Robot.*, vol. 25, no. 5, pp. 985–994, Oct. 2009.

[28] R. Schlanbusch, R. Kristiansen, and P. J. Nicklasson, "Spacecraft formation reconfiguration with collision avoidance," *Automatica*, vol. 47, pp. 1443–1449, Jul. 2011.

[29] Y. Koren and J. Borenstein, "Potential field methods and their inherent limitations for mobile robot navigation," in *Proc. IEEE Int. Conf. Robot. Automat.*, vol. 2, Sacramento, CA, USA, Apr. 1991, pp. 1398–1404.

[30] X. Zhu, X.-X. Zhang, M.-D. Yan, Y.-H. Qu, and H. Lin, "Three-dimensional multiple unmanned aerial vehicles formation control strategy based on second-order consensus," *Proc. Inst. Mech. Eng., G, J. Aerosp. Eng.*, vol. 232, no. 3, pp. 481–491, 2018.

[31] W. Ren and R. W. Beard, "Consensus seeking in multiagent systems under dynamically changing interaction topologies," *IEEE Trans. Autom. Control*, vol. 50, no. 5, pp. 655–661, May 2005.

[32] H. Liu, H. Fang, Y. Mao, H. Cao, and R. Jia, "Distributed flocking control and obstacle avoidance for multi-agent systems," in *Proc. 29th Chin. Control Conf.*, Beijing, China, Jul. 2010, pp. 4536–4541.
[33] M. R. D'Orsogna, Y. L. Chuang, A. L. Bertozzi, and L. S. Chayes, "Self-propelled particles with soft-core interactions: Patterns, stability, and collapse," *Phys. Rev. Lett.*, vol. 96, no. 10, 2006, Art. no. 104302.
[34] G. Antonelli, F. Arrichiello, and S. Chiaverini, "The null-space-based behavioral control for soccer-playing mobile robots," in *Proc. IEEE/ASME Int. Conf. Adv. Intell. Mechtron.*, vol. 2. Monterey, CA, USA: AIAA, Jul. 2005, pp. 1257–1262.

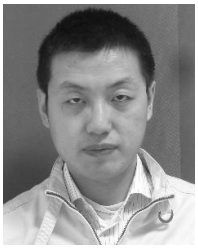

XU ZHU received the M.S. and Ph.D. degrees in control theory and control engineering from Northwestern Polytechnical University, China, in 2014. He is currently an Associate Professor with the School of Electronic and Control Engineering, Chang'an University, China. His research interests are multi-UAV cooperative control, fight control, and automated vehicular platoon control.

YUFEI LIANG received the B.S. degree in information and computing science from the East China University of Technology, China, in 2016. He is currently pursuing the M.S. degree in control theory and control engineering with Chang'an University, China. His research interests include multi-UAV cooperative control and fight control.

MAODE YAN received the M.S. and Ph.D. degrees in control theory and control engineering from Northwestern Polytechnical University, China, in 1999 and 2001, respectively. He is currently a Professor with the School of Electronic and Control Engineering, Chang'an University, China. His research interests are networked control systems, robots and their formation control, and embedded systems and applications.